mathematics

MDPI

Article

The Effect of Fractional Time Derivative on Two-Dimension Porous Materials Due to Pulse Heat Flux

Tareq Saeed [1] and Ibrahim A. Abbas [1,2,*]

[1] Mathematics Department, Faculty of Science, King Abdulaziz University, Jeddah 21589, Saudi Arabia; tsalmalki@kau.edu.sa
[2] Department Mathematics, Faculty of Science, Sohag University, Sohag 82524, Egypt
* Correspondence: ibrabbas7@science.sohag.edu.eg

Abstract: In the present article, the generalized thermoelastic wave model with and without energy dissipation under fractional time derivative is used to study the physical field in porous two-dimensional media. By applying the Fourier-Laplace transforms and eigenvalues scheme, the physical quantities are presented analytically. The surface is shocked by heating (pulsed heat flow problem) and application of free traction on its outer surface (mechanical conditions) by the process of temperature transport (diffusion) to observe the full analytical solutions of the main physical fields. The magnesium (Mg) material is used to make the simulations and obtain numerical outcomes. The basic physical field quantities are graphed and discussed. Comparisons are made in the results obtained under the strong (SC), the weak (WC) and the normal (NC) conductivities.

Keywords: Fourier-Laplace transforms; porous material; eigenvalues method; fractional time derivative

Citation: Saeed, T.; A. Abbas, I. The Effect of Fractional Time Derivative on Two-Dimension Porous Materials Due to Pulse Heat Flux. *Mathematics* **2021**, *9*, 207. https://doi.org/10.3390/math9030207

Academic Editor: Snezhana Hristova
Received: 21 December 2020
Accepted: 14 January 2021
Published: 20 January 2021

1. Introduction

Porous media appear in many forms of environmental, natural, and synthetic implementations and in several technologies. To overcome the first insufficiency in the decoupled thermoelasticity theorem, in 1956, Biot [1] presented the coupled thermoelasticity theorem to control the first insufficiency in the decoupled thermoelastic model, which prognosticates two phenomena not suitable for physical observation. Firstly, the thermal conductivity equation is parabolic, presenting an infinite propagation speed for thermal waves. Secondly, the thermal conductivity equation of this model does not contain an elastic term. Rosencwaig et al. [2] investigated the local thermoelastic deformation of the model caused by excitations.

Biot developed poroelasticity models [1,3,4] for a high–low-frequency range and built upon the coupled thermoelasticity hypothesis to overcome the inconsistency in the uncoupled hypothesis [1]. The heat conduction and elasticity equations in this theory are coupled. However, it includes a drawback of the uncoupled hypothesis in which the heat wave propagates with an infinite velocity that is impractical in nature. Then, to solve the problem of the coupled hypothesis, generalized thermoelasticity models were expanded. It is recognized that there are several generalizations of the thermoelasticity hypothesis, such as that presented by Lord-Shulman [5]. Green-Naghdi [6–8] formulated three types of models (GNI, GNII, and GNIII). The constitutive equations of the GN models are linearized, where the first type is similar to the classical coupled thermoelastic model, the second type demonstrates the propagations of thermal signals with finite velocity without energy dissipations, and the third type proposes the finite speed of propagations with energy dissipations. During the second half of the 19th century, it can be said that the complete model of fractional integrals and derivatives was determined. In the context of generalized thermoelastic models, Youssef [9,10] established generalized fractional-order thermoelastic models under strong, normal, and weak conductivities. Sherief et al. [11] presented a new theory by using the thermal conduction law. Ezzat and Elkaramany [12] established

another theory for a generalized fractional-order thermoelasticity model based on Taylor's expansions of time-fractional order. Ezzat et al. [13] studied modeling in a generalized thermoelastic model using a memory-dependent derivative. Marin [14] discussed basic models in elastostatic micropolar media. Saeed et al. [15] used the finite-element scheme to investigate thermoelastic interactions in poroelastic media using the GL model.

Ouyang et al. [16] proposed three-equation models considering local thermal nonequilibrium states. Many authors [17–23] have discussed the solutions to some problems using various generalized thermoelastic models. Hussein [24] presented a mathematical model for a spherical thermoelastic porous material. Hobiny and Abbas [25] discussed the effect of a dual-phase lag model in two-dimensional porous media. Biswas [26] investigated surface waves in nonlocal, orthotropic thermoelastic porous media. Carini and Zampoli [27] studied porous matrices with three delay times. Abbas and Marin [28] presented the analytical solution of a two-dimensional generalized thermodiffusion problem subjected to a laser pulse. Shekhar [29] studied deformations caused by thermal shock in a porous thermoelastic medium with properties dependent on the reference temperature. Calin et al. [30] investigated improvements in the rigidity of circular-plate composites. Abd-Elaziz et al. [31] discussed the Thomson impacts on thermoelastic porous materials based on Green and Naghdi's model. Abbas and Kumar [32] investigated deformations induced by a heating source in the micropolar plane under generalized thermoelasticity using the finite-element scheme.

Ellahi et al. [33,34] studied the solutions of different problems under several boundary conditions in porous media. Singh [35] has investigated the wave propagations in a medium with voids under thermoelasticity models. Palani and Abbas [36] discussed the free convections magnetohydrodynamics flow with thermal radiations. Villatoro et al. [37] have applied the perturbation approach upon Laplace transform to get the solution of the heating equation in porous media which consists of gas and solid phases. The discontinuous front was observed in gas temperature because of incompatibility between the initial and boundary conditions, leading to the constant speed for thermal propagation. However, there was a smooth front at the solid temperature using an internal layer of asymptotic approximation. Abbas [38] discussed the natural frequency of a poro-elastic hollow cylinders. Alzahrani et al. [39] used the eigenvalues approaches to investigate the effects of thermal relaxation times in two-dimension porous media under strong, normal and weak thermal conductivities.

The objective of this work is to study the effects of strong, weak, and normal conductivities in a two-dimensional porous medium by using the eigenvalue scheme. By using the eigenvalue technique with Fourier–Laplace transforms on numerical and analytical methods, basic formulations are presented. The nondimensional temperature, displacements, stresses, and volume fraction are obtained and represented graphically. In the calculations, the impacts of strong, normal, and weak thermal conductivities on the considered variables are investigated and compared.

2. Basic Equations

For an isotropic 2D elastic porous material, the basic formulations based on [9,35] models without body force and the heating resources are expressed as:

$$(\lambda + \mu)u_{j,ij} + \mu u_{i,jj} + b\varphi_{,i} - \gamma_t \Theta_{,i} = \rho \frac{\partial^2 u_i}{\partial t^2}, \tag{1}$$

$$\alpha \varphi_{,jj} - b u_{j,j} - \zeta_1 \varphi - \omega_o \frac{\partial \varphi}{\partial t} + m\Theta = \rho \psi \frac{\partial^2 \varphi}{\partial t^2}, \tag{2}$$

$$\left(\left(K^* + K \frac{\partial}{\partial t} \right) I^{\epsilon - 1} \Theta_{,j} \right)_{,j} = \frac{\partial}{\partial t} \left(\rho c_e \frac{\partial \Theta}{\partial t} + m T_o \varphi + \gamma_t T_o \frac{\partial u_{j,j}}{\partial t} \right), \tag{3}$$

where the integral operator of fractional derivative is expressed as [9]

$$I^{\epsilon-1}g(\boldsymbol{r},t)=\frac{1}{\Gamma(\in)}\int_0^t(t-\tau)^{\epsilon-1}g(\boldsymbol{r},\tau)d\tau,\begin{cases}0<\epsilon<1, & \textit{weak conductivity}\\ \epsilon=1, & \textit{normal conductivity},\\ 1<\epsilon\leq 2, & \textit{strong conductivity}\end{cases}\tag{4}$$

where $\Gamma(\in)$ is the Gamma function. The stress-displacement equations are defined by [35]

$$\sigma_{ij}=\mu\left(u_{i,j}+u_{j,i}\right)+(\lambda u_{k,k}+b\varphi-\gamma_t\Theta)\delta_{ij}.\tag{5}$$

where m is the coefficient of thermo-void, ψ is the equilibrated inertia, b is the measure of diffusion effects, ω_o, α,ζ_1 are the parameters of voids material, c_e is the specific heat, K^* is the model characteristic material constant, $\Theta=T-T_o$, T_o is the reference temperature, ρ is the material density, σ_{ij} are the stress components, K is the thermal conductivity coefficient, μ,λ are the Lame's parameters, t is the time, u_i are the components of displacement, $i,j,k=1,2,3$, $\gamma_t=(3\lambda+2\mu)\alpha_t$, α_t is the linear coefficient of thermal expansions.

3. Formulations of the Problem

We consider a two-dimension porous material fills the region $0\leq x\leq\infty$, $-\infty\leq y\leq\infty$. By using the Cartesian co-ordinates (x,y,z), the governing equations with the components of the displacement $(u,v,0)$ can be given by

$$(\lambda+2\mu)\frac{\partial^2u}{\partial x^2}+(\lambda+\mu)\frac{\partial^2v}{\partial x\partial y}+\mu\frac{\partial^2u}{\partial y^2}+b\frac{\partial\varphi}{\partial x}-\gamma_t\frac{\partial\Theta}{\partial x}=\rho\frac{\partial^2u}{\partial t^2}\tag{6}$$

$$(\lambda+2\mu)\frac{\partial^2v}{\partial y^2}+(\lambda+\mu)\frac{\partial^2u}{\partial x\partial y}+\mu\frac{\partial^2v}{\partial x^2}+b\frac{\partial\varphi}{\partial y}-\gamma_t\frac{\partial\Theta}{\partial y}=\rho\frac{\partial^2v}{\partial t^2},\tag{7}$$

$$\alpha\left(\frac{\partial^2\varphi}{\partial x^2}+\frac{\partial^2\varphi}{\partial y^2}\right)-\omega_o\frac{\partial\varphi}{\partial t}-\zeta_1\varphi-b\left(\frac{\partial u}{\partial x}+\frac{\partial v}{\partial y}\right)+m\Theta=\rho\psi\frac{\partial^2\varphi}{\partial t^2},\tag{8}$$

$$\left(K^*+K\frac{\partial}{\partial t}\right)I^{\epsilon-1}\left(\frac{\partial^2\Theta}{\partial x^2}+\frac{\partial^2\Theta}{\partial y^2}\right)=\frac{\partial}{\partial t}\left(\rho c_e\frac{\partial\Theta}{\partial t}+mT_o\varphi+\gamma_tT_o\frac{\partial}{\partial t}\left(\frac{\partial u}{\partial x}+\frac{\partial v}{\partial y}\right)\right),\tag{9}$$

$$\sigma_{xx}=\lambda\frac{\partial v}{\partial y}+(\lambda+2\mu)\frac{\partial u}{\partial x}+b\varphi-\gamma_t\Theta,\ \sigma_{xy}=\mu\left(\frac{\partial u}{\partial y}+\frac{\partial v}{\partial x}\right).\tag{10}$$

The problem initial conditions are defined by

$$\varphi=\frac{\partial\varphi}{\partial t}=0,\Theta=\frac{\partial\Theta}{\partial t}=0,\ u=\frac{\partial u}{\partial t}=0,\ v=\frac{\partial v}{\partial t}=0,t=0.\tag{11}$$

While, the problem boundary conditions are given by

$$\sigma_{xx}=0,\sigma_{xy}=0,-\left(K^*+K\frac{\partial}{\partial t}\right)\frac{\partial\Theta(x,y,t)}{\partial x}=q_o\frac{t^2e^{-\frac{t}{t_p}}}{16t_p^2}H(a-|y|),\ \frac{\partial\varphi}{\partial x}=0\tag{12}$$

where q_o is a constant, t_p is the time of the flux pulse heating characteristics, and H is the function unit step. For appropriateness, the nondimensional variables can be taken as

$$\Theta'=\frac{\Theta}{T_o},\ \varphi'=\psi\eta^2c^2\varphi,\ \left(\sigma'_{xx},\sigma'_{xy}\right)=\frac{\left(\sigma_{xx},\ \sigma_{xy}\right)}{(\lambda+2\mu)},\left(t',t'_p\right)=\eta c^2(t,t_p),\ (u',v',x',y')=\eta c(u,v,x,y),\tag{13}$$

where $\eta=\frac{\rho c_e}{k}$ and $c=\sqrt{\frac{\lambda+2\mu}{\rho}}$. In these nondimensional terms of the variables in Equation (13), the basic formulations can be written by (the dashes have been neglected for convenience)

$$\frac{\partial^2u}{\partial t^2}=\frac{\partial^2u}{\partial x^2}+(1-r_1)\frac{\partial^2v}{\partial x\partial y}+r_1\frac{\partial^2u}{\partial y^2}+r_2\frac{\partial\varphi}{\partial x}-r_3\frac{\partial\Theta}{\partial x},\tag{14}$$

$$\frac{\partial^2 v}{\partial t^2} = \frac{\partial^2 v}{\partial y^2} + (1 - r_1)\frac{\partial^2 u}{\partial x \partial y} + r_1 \frac{\partial^2 v}{\partial x^2} + r_2 \frac{\partial \varphi}{\partial y} - r_3 \frac{\partial \Theta}{\partial y}, \tag{15}$$

$$r_4 \frac{\partial^2 \varphi}{\partial t^2} = \frac{\partial^2 \varphi}{\partial x^2} + \frac{\partial^2 \varphi}{\partial y^2} - r_5 \frac{\partial \varphi}{\partial t} - r_6 \varphi - r_7 \left(\frac{\partial u}{\partial x} + \frac{\partial v}{\partial y} \right) + r_8 \Theta, \tag{16}$$

$$\left(r_9 + \frac{\partial}{\partial t} \right) \left(\frac{\partial^2 \Theta}{\partial x^2} + \frac{\partial^2 \Theta}{\partial y^2} \right) = \frac{\partial^\epsilon}{\partial t^\epsilon} \left(\frac{\partial \Theta}{\partial t} + r_{10} \varphi + r_{11} \frac{\partial}{\partial t} \left(\frac{\partial u}{\partial x} + \frac{\partial v}{\partial y} \right) \right), \tag{17}$$

$$\sigma_{xx} = (1 - 2r_1)\frac{\partial v}{\partial y} + \frac{\partial u}{\partial x} + r_2 \varphi - r_3 \Theta, \; \sigma_{xy} = r_1 \left(\frac{\partial v}{\partial x} + \frac{\partial u}{\partial y} \right). \tag{18}$$

$$\sigma_{xx} = \sigma_{xy} = 0.0, \; \left(r_9 + \frac{\partial}{\partial t} \right) \frac{\partial \Theta(x, y, t)}{\partial x} = -q_o \frac{t^2 e^{-\frac{t}{t_p}}}{16 t_p^2} H(a - |y|), \; \frac{\partial \varphi}{\partial x} = 0, \tag{19}$$

where $r_1 = \frac{\mu}{\rho c^2}$, $r_2 = \frac{b}{\rho \psi \eta^2 c^4}$, $r_3 = \frac{\gamma_t T_o}{\rho c^2}$, $r_4 = \frac{\rho c^2 \psi}{\alpha}$, $r_5 = \frac{\omega_o}{\alpha \eta}$, $r_6 = \frac{\zeta_1}{\alpha \eta^2 c^2}$, $r_7 = \frac{b \psi}{\alpha}$, $r_8 = \frac{m \psi T_o}{\alpha}$, $r_9 = \frac{K^*}{\rho c_e c^2}$, $r_{10} = \frac{m}{\psi \eta^4 c^4 k}$, $r_{11} = \frac{\gamma_t}{\rho c_e}$.

Now, the Laplace transforms for any function $f(x, y, t)$, are given by

$$\overline{f}(x, y, s) = \int_0^\infty f(x, y, t) e^{-st} dt, \tag{20}$$

however, the Fourier transform for any function $\overline{f}(x, y, s)$ can be expressed by

$$\overline{f}^*(x, q, s) = \int_{-\infty}^\infty \overline{f}(x, y, s) e^{-iqy} dy, \tag{21}$$

Thus, the governing formulations are expressed to obtain the ordinary differential equations with the boundary conditions as follow

$$\frac{d^2 \overline{u}^*}{dx^2} = \left(s^2 + r_1 q^2 \right) \overline{u}^* - iq(1 - r_1) \frac{d\overline{v}^*}{dx} - r_2 \frac{d\overline{\varphi}^*}{dx} + r_3 \frac{d\,\overline{\Theta}^*}{dx}, \tag{22}$$

$$\frac{d^2 \overline{v}^*}{dx^2} = \frac{(s^2 + q^2)}{r_1} \overline{v}^* - \frac{r_2 iq}{r_1} \overline{\varphi}^* + \frac{r_3 iq}{r_1} \overline{\Theta}^* - \frac{iq(1 - r_1)}{r_1} \frac{d\overline{u}^*}{dx}, \tag{23}$$

$$\frac{d^2 \overline{\varphi}^*}{dx^2} = r_7 iq \overline{v}^* + \left(s^2 r_4 + q^2 + r_6 + r_5 s \right) \overline{\varphi}^* - r_8 \overline{\Theta}^* + r_7 \frac{d\overline{u}^*}{dx}, \tag{24}$$

$$\frac{d^2\,\overline{\Theta}^*}{dx^2} = \frac{r_{11} iq s^{\in+1}}{r_9 + s} \overline{v}^* + \frac{r_{10} s^{\in}}{r_9 + s} \overline{\varphi}^* + \left(q^2 + \frac{s^{\in+1}}{r_9 + s} \right) \overline{\Theta}^* + \frac{s^{\in+1} r_{11}}{r_9 + s} \frac{d\overline{u}^*}{dx}, \tag{25}$$

$$\overline{\sigma}_{xx}^* = iq(1 - 2r_1)\overline{v}^* + \frac{d\overline{u}^*}{dx} + r_2 \overline{\varphi}^* - r_3 \overline{\Theta}^*. \tag{26}$$

$$\overline{\sigma}_{xy}^* = r_1 \left(\frac{d\overline{v}^*}{dx} + iq\overline{u}^* \right), \tag{27}$$

$$\overline{\sigma}_{xx}^* = \overline{\sigma}_{xy}^* = 0, \frac{d\overline{\varphi}^*}{dx} = 0, \frac{d\,\overline{\Theta}^*}{dx} = -\frac{q_o t_p}{8(r_9 + s)(s t_p + 1)^3} \sqrt{\frac{2}{\pi}} \frac{sin(qa)}{q}, \tag{28}$$

Now, the vector-matrix differential equations (Equations (22)–(25)) are written as

$$\frac{dM}{dx} = AM, \tag{29}$$

where A and M are defined as shown in Appendix A. By using the eigenvalues method as in [17,40–43], the exact solutions for the Equation (29) are obtained. So, the matrix characteristic equation for A are taken the form as follow:

$$\xi^8 - f_1 \xi^6 + f_2 \xi^4 + f_3 \xi^2 + f_4 = 0, \tag{30}$$

where f_1, f_2, f_3 and f_4 are determined as in Appendix B. To obtain the solution of Equation (29), the eigenvalue of matrix A and its eigenvectors must be computed, where ξ_1, ξ_2, ξ_3, ξ_4, $-\xi_1$, $-\xi_2$, $-\xi_3$ and $-\xi_4$ are the eigenvalues which have the corresponding eigenvectors as in Appendix C. Thus, the analytical solutions of Equation (29) are written as:

$$M(x,q,s) = \sum_{i=1}^{4} B_i Y_i e^{-\xi_i x}, \tag{31}$$

The positive exponentials can be discarded, which, due to the conditions of the regulations of the solution at infinity and B_1, B_2, B_3, and B_4, are constants that are computed using the conditions of the problem boundary. Now, for each function $\overline{f}^*(x, q, s)$, the inverse Fourier transform can be expressed by

$$\overline{f}(x,y,s) = \frac{1}{\sqrt{2\pi}} \int_{-\infty}^{\infty} \overline{f}^*(x,q,s) e^{iqy} dq, \tag{32}$$

Finally, to get the general solution for the displacement, the stresses components, the changes in volume fraction field of void distributions φ and the variations of temperature with respect to the distances x, y at any time t, Stehfest [44] numerical inversion schemes were chosen. In these schemes, the Laplace transform inverse for $\overline{f}(x,y,s)$ are defined by

$$f(x,y,t) = \frac{ln(2)}{t} \sum_{n=1}^{N} V_n \overline{f}\left(x, y, n\frac{ln(2)}{t}\right), \tag{33}$$

where

$$V_n = (-1)^{\left(\frac{N}{2}+1\right)} \sum_{p=\frac{n+1}{2}}^{min(n,\frac{N}{2})} \frac{(2p)! p^{(1+\frac{N}{2})}}{p!(n-p)!\left(\frac{N}{2}-p\right)!(2n-1)!}, \tag{34}$$

where N is the term number.

4. Numerical Results

For numerical examples, the magnesium mediums can be taken to object of numerical calculations. The parameters values of (Mg) are taken from [45]

$$\alpha = 3.688 \times 10^{-5}(\mathrm{N}),\ \zeta_1 = 1.475 \times 10^{10}(\mathrm{N})\left(\mathrm{m}^{-2}\right), \omega_o = 0.0787 \times 10^{-3}(\mathrm{N})\left(\mathrm{m}^{-2}\right)\left(\mathrm{s}^{-1}\right),$$
$$\mu = 3.278 \times 10^{10}(\mathrm{N})\left(\mathrm{m}^{-2}\right),\ \lambda = 2.17 \times 10^{10}(\mathrm{N})\left(\mathrm{m}^{-2}\right), \rho = 1740(\mathrm{kg})\left(\mathrm{m}^{-3}\right),\ t = 0.3,$$
$$T_o = 298(\mathrm{k}),\ c_e = 1040\ (\mathrm{J})\left(\mathrm{kg}^{-1}\right)\left(\mathrm{k}^{-1}\right),\ a = 0.25,\ \psi = 1.753 \times 10^{-15}\left(\mathrm{m}^2\right),$$
$$\alpha_t = 1.98 \times 10^{-6}\left(\mathrm{k}^{-1}\right), K = 1.7\ (\mathrm{W})\left(\mathrm{k}^{-1}\right)\left(\mathrm{m}^{-1}\right),\ \beta = 2.68 \times 10^{6}(\mathrm{N})\left(\mathrm{m}^{-2}\right)\left(\mathrm{k}^{-1}\right),$$
$$b = 1.13840 \times 10^{10}(\mathrm{N})\left(\mathrm{m}^{-2}\right), m = 2 \times 10^{6}(\mathrm{N})\left(\mathrm{m}^{-2}\right)\left(\mathrm{k}^{-1}\right).$$

The above data have been used to study the strong (SC), the normal (NC) and the weak (WC) conductivities in 2D porous materials by the eigenvalue method. The voids changes in volume fraction field distribution φ, The variations of temperature Θ, the stresses σ_{xx}, σ_{xy} and the of displacement components u, v are studied. The material is considered to be homogeneous two-dimensions media. Figure 1 displays the change in the volume fraction field of void distributions φ along x. It is clear that it reduces with the rising x till attaining zeros. Figure 2 displays the temperature variations via x. It is noticed that it starts from heights value according to the application of boundary condition and reduces with the rising x to come to zeros. Figure 3 depicts the variations of vertical displacement with respect to x which have maximum value on $x = 0$ and reduces with the rising x. Figure 4 illustrates the horizontal displacement variations u via x. It is indicated that it attains maximums negative value and gradually rises till it attains peak value at specific locations in close nearness to $x = 0$ and after that reduces to come to zeros. As seen in Figure 4, the displacement changes continuously from negative to positive and after that goes down to zero, which is caused by the combined effect of the traction free bounding

surface, thermal expansion and finite heat speed. Figures 5 and 6 show the components of stress variations σ_{xy} and σ_{xx} along x. It is noticed that the magnitudes of components, permanently begin from zeros which obeyed the boundary condition.

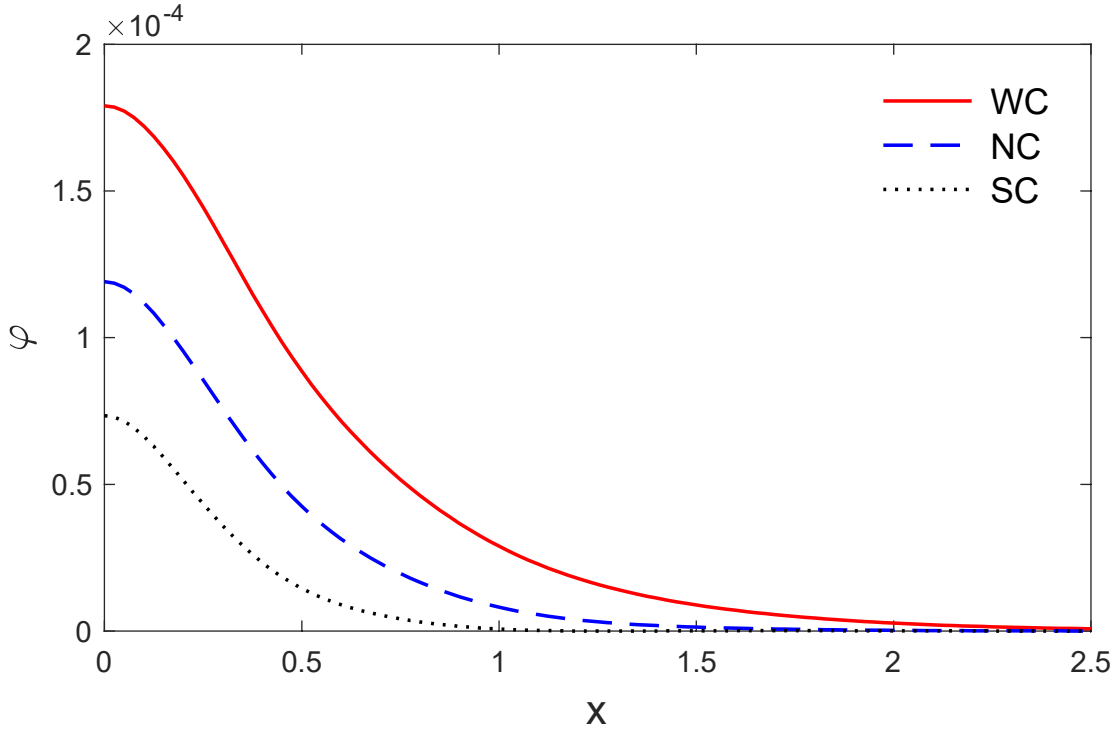

Figure 1. The change in volume fraction field of void variations φ via x and $y = 0.4$ for strong normal and weak conductivities.

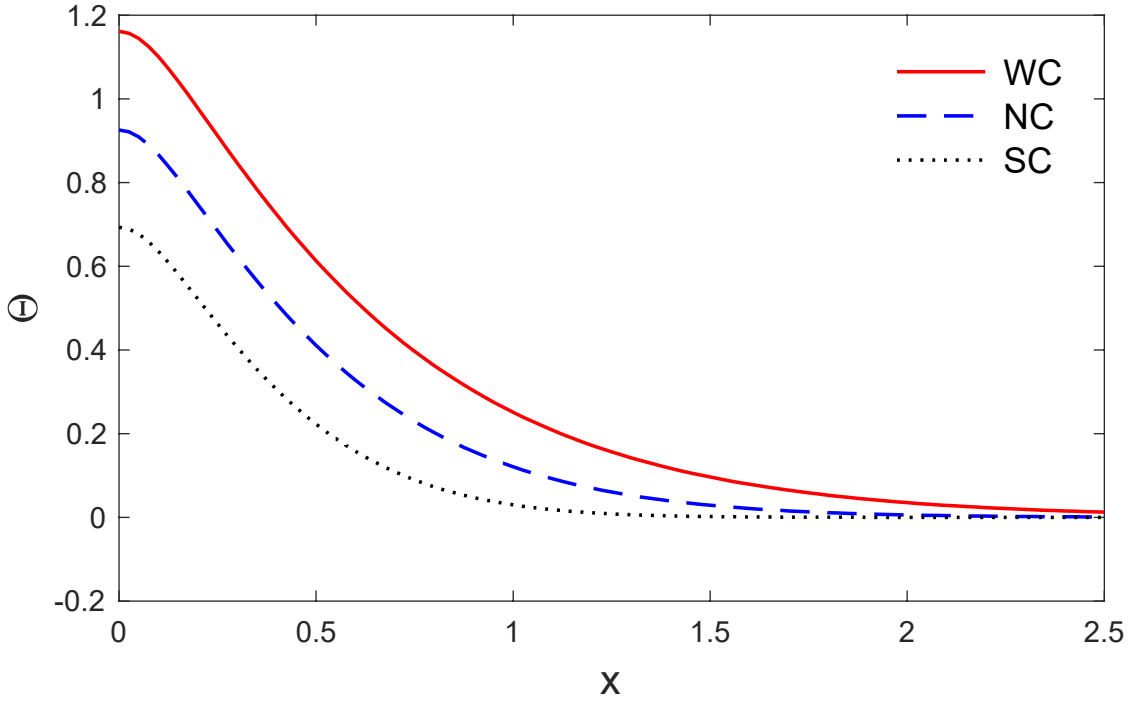

Figure 2. The variation of temperature Θ via x and $y = 0.4$ for strong normal and weak conductivities.

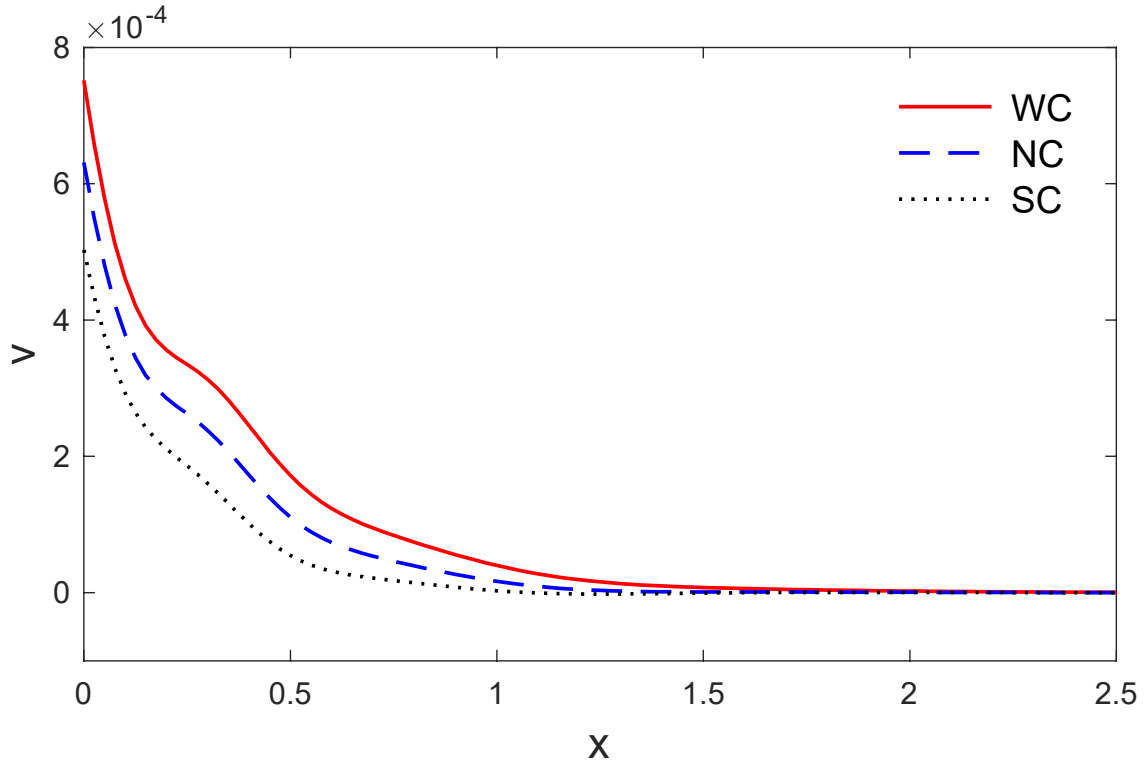

Figure 3. The variations of vertical displacement v via x with $y = 0.4$ for strong normal and weak conductivities.

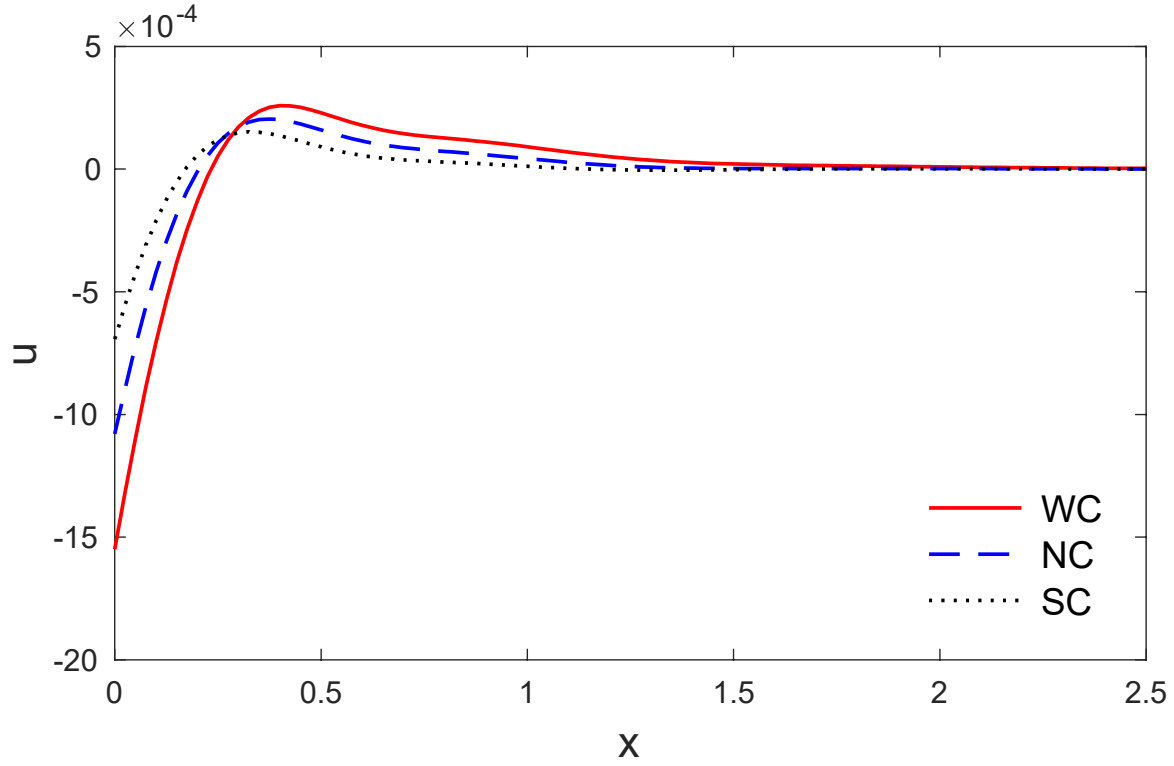

Figure 4. The variations of horizontal displacement u via x with $y = 0.4$ for strong normal and weak conductivities.

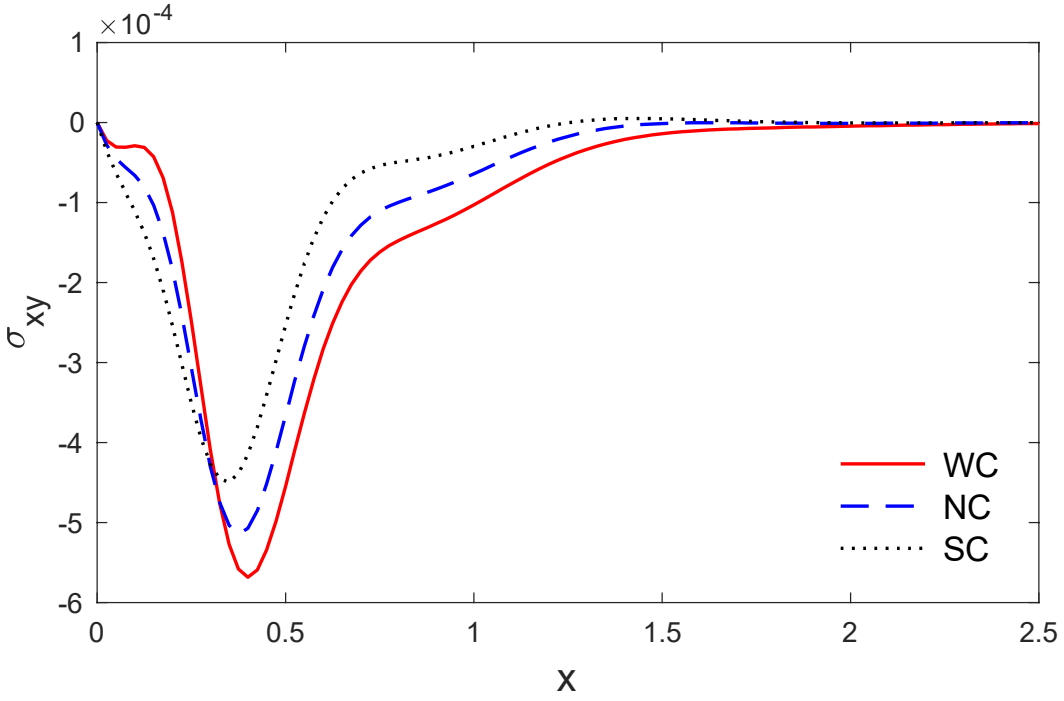

Figure 5. The variation of stress σ_{xy} via x with $y = 0.4$ for strong normal and weak conductivities.

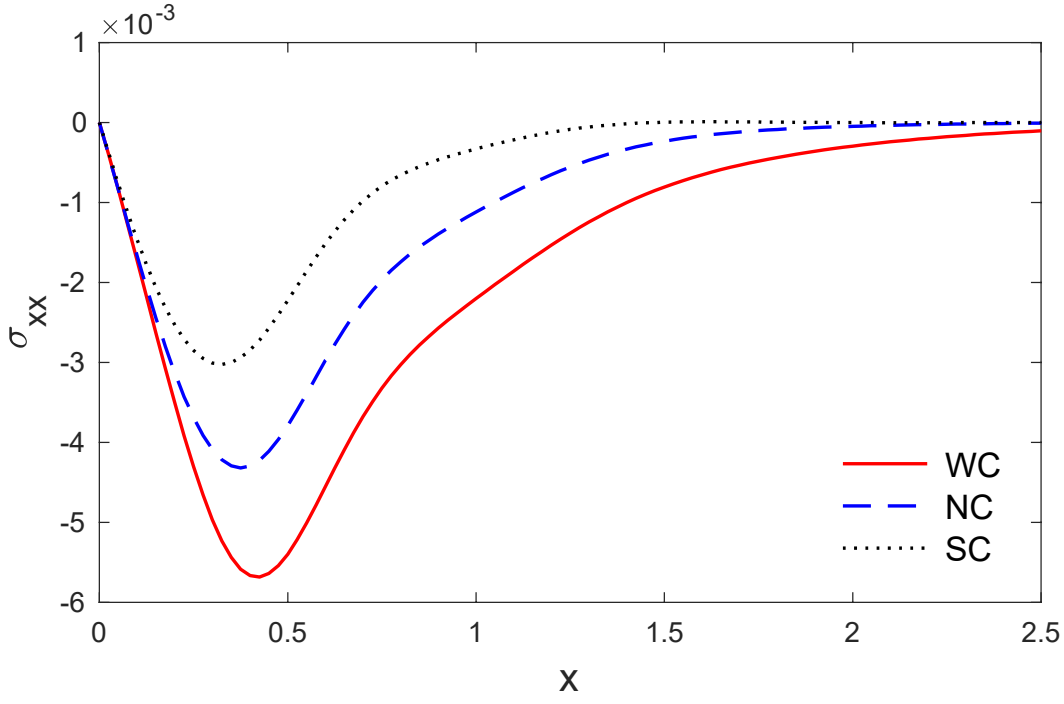

Figure 6. The variation of stress σ_{xx} via x and $y = 0.4$ for strong normal and weak conductivities.

Figures 7 and 8 show the changes in volume fraction field of voids variations φ and the variations of temperature Θ via the distance y when $x = 0.4$. It is indicated that the variations of changes in volume fraction field of void and the variations of temperature have maximum values at the length of heating surfaces $((|y| \leq 0.4))$ after that begin to reduces totally near the edges $((|y| \leq 0.4))$ where they reduce and reach to zeros values. Figure 9 displays the vertical displacement variation v via y. It is noticed that it starts the rising at the start and end of the thermal surfaces $(|y| \leq 0.4)$, and have small values

at the center of the thermal surfaces ($|y| \leq 0.4$), after that it begins the rising and reach ultimate value totally near the edges ($y = \pm 0.4$), then it reduces to come to zeros. Figure 10 shows the variation of horizontal displacement u along x. It is observed that the horizontal displacement has a maximum value at the length of the heating surface ($|y| \leq 0.4$), and then it starts to decrease totally near the edges ($y = \pm 0.4$), and then reduces to zeros values. The stresses σ_{xx} and σ_{xy} with respect to y are presented in Figures 11 and 12.

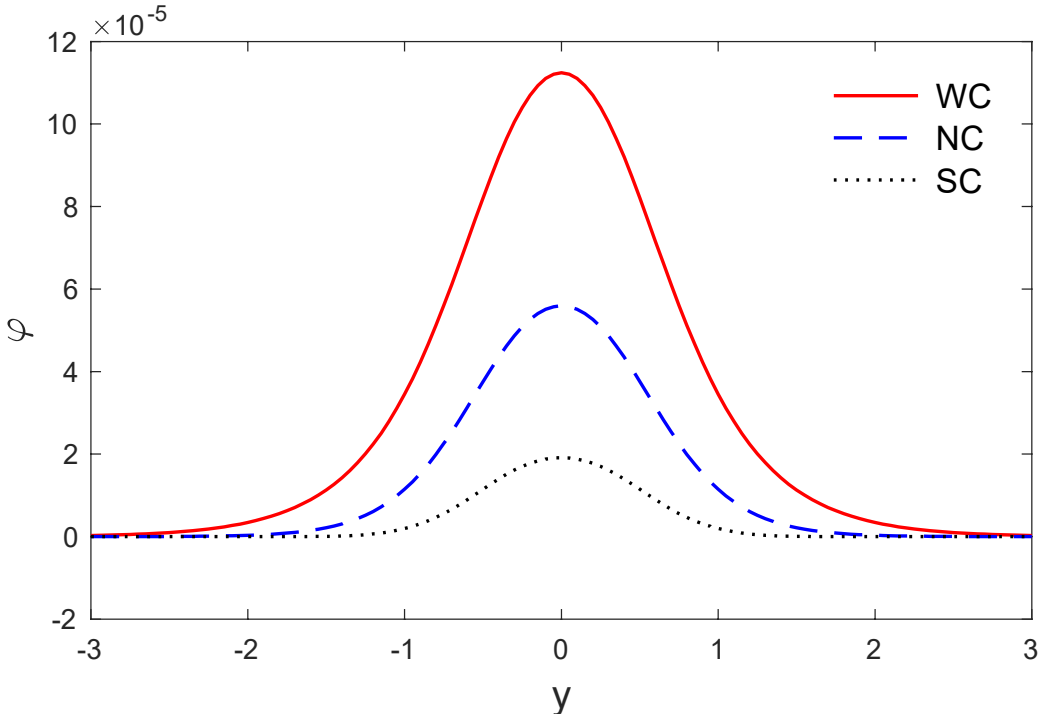

Figure 7. The change in volume fraction field of void variations φ via y and $x = 0.4$ for strong normal and weak conductivities.

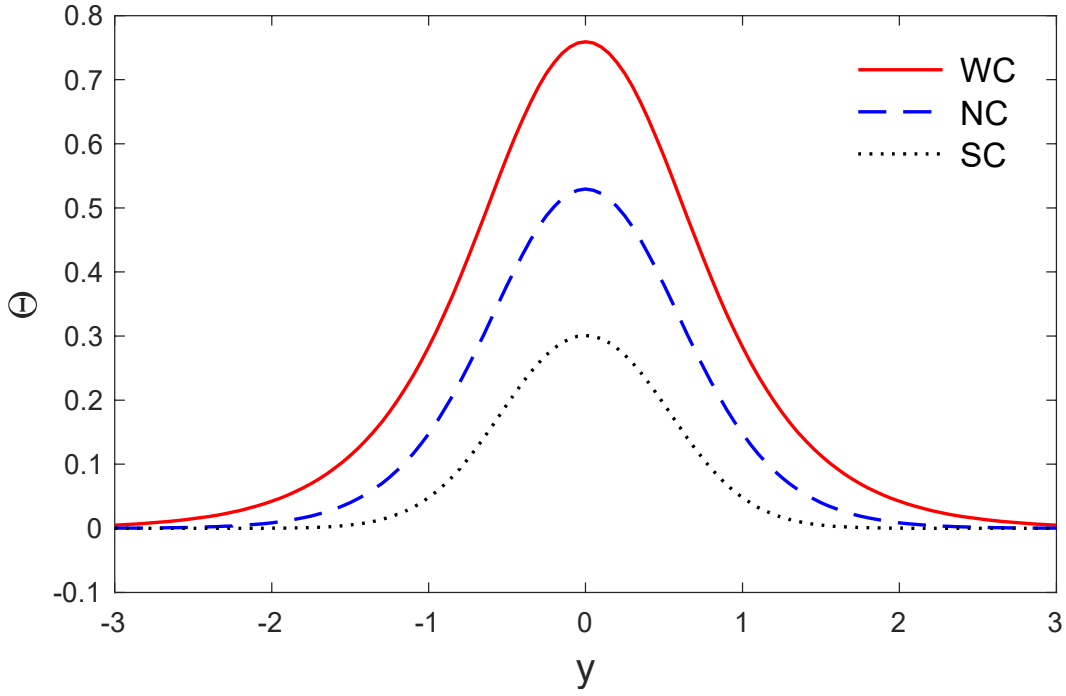

Figure 8. The variations of temperature Θ via y and $x = 0.4$ for strong normal and weak conductivities.

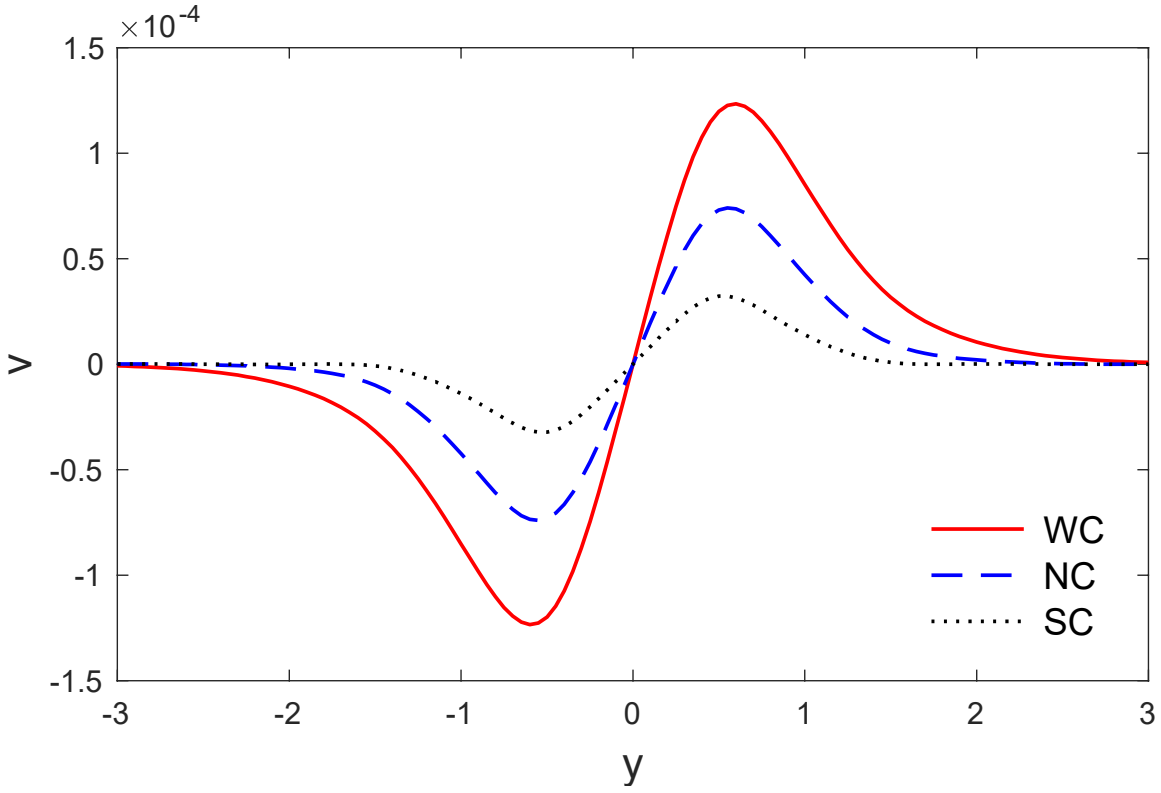

Figure 9. The variations of vertical displacement v via y with $x = 0.4$ for strong normal and weak conductivities.

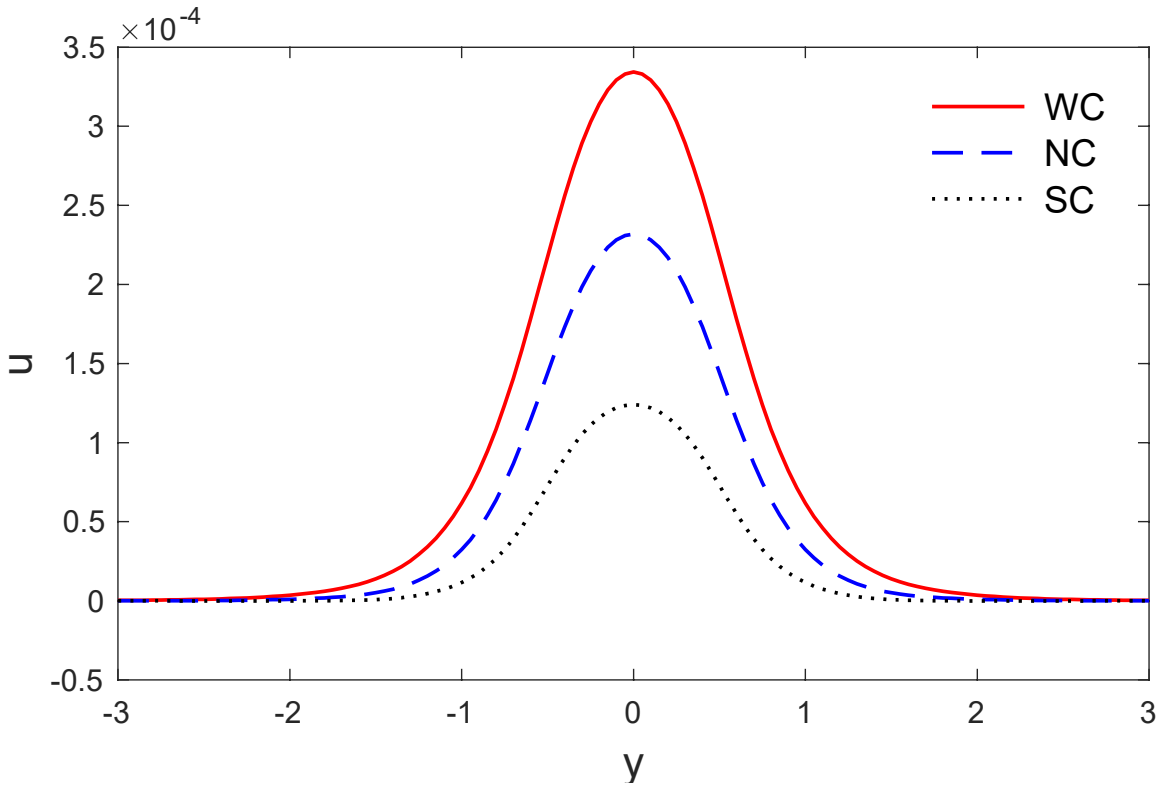

Figure 10. The variations of horizontal displacement u via y with $x = 0.4$ for strong normal and weak conductivities.

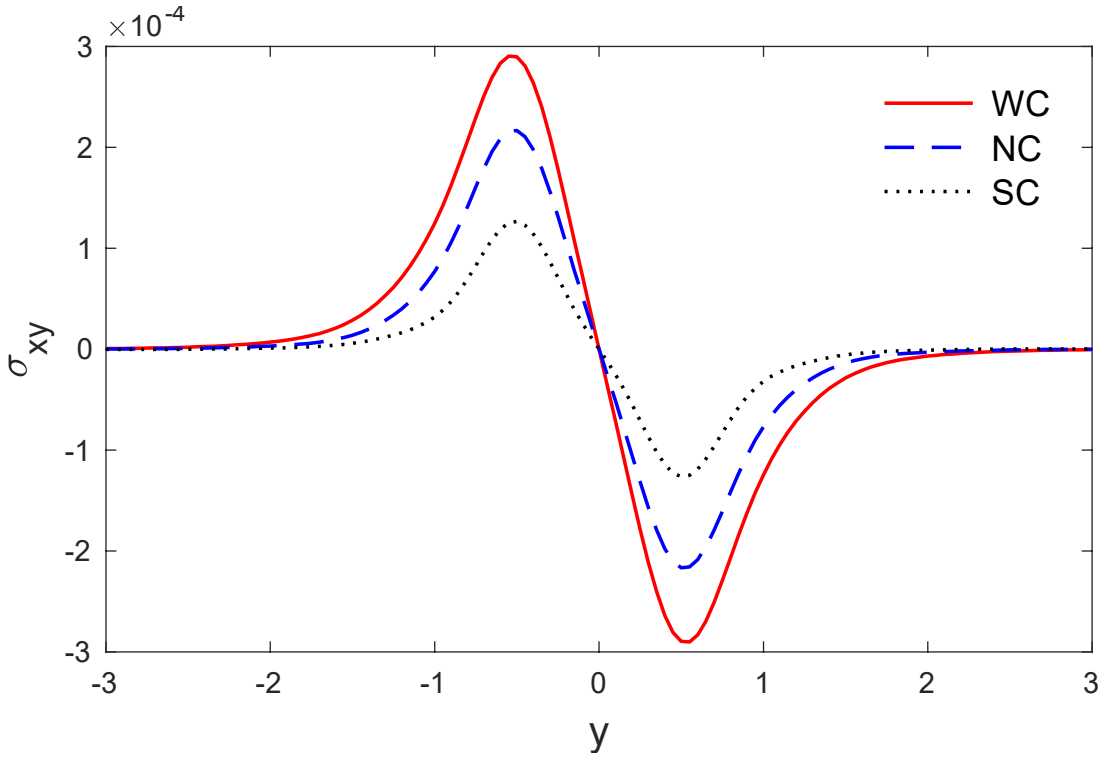

Figure 11. The variation of stresses component σ_{xy} versus y when $x = 0.4$ for strong normal and weak conductivities.

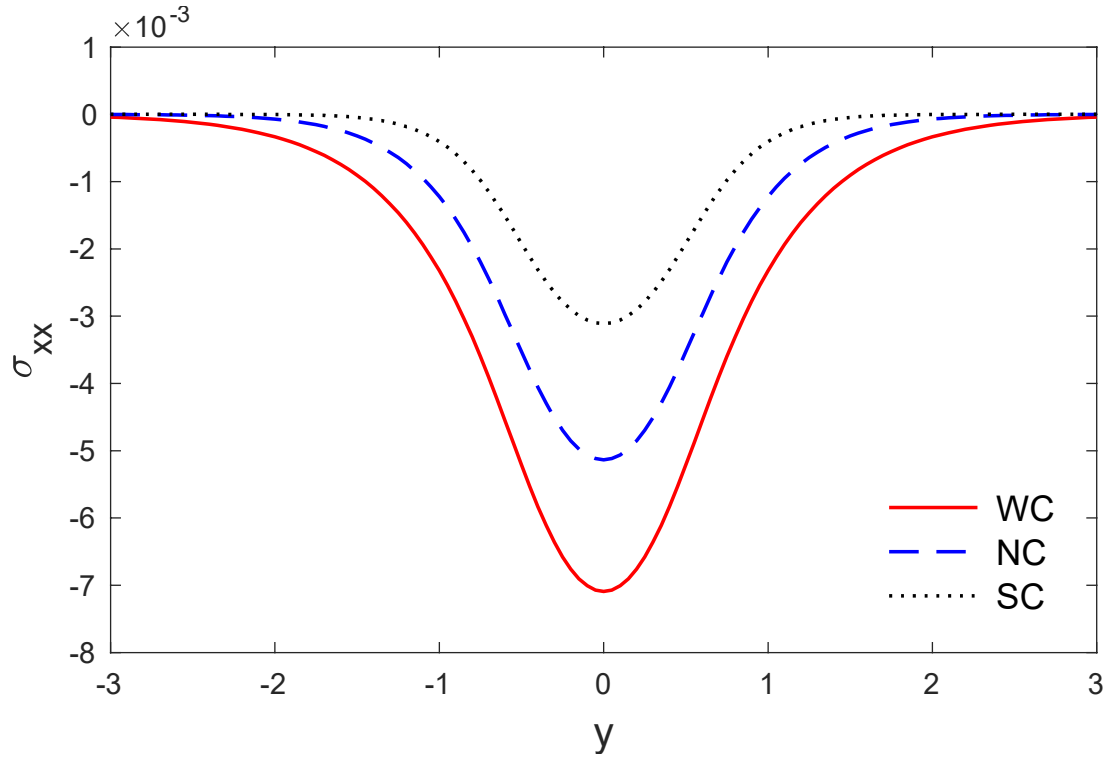

Figure 12. The variation of stresses components σ_{xx} versus y when $x = 0.4$ for strong normal and weak conductivities.

Finally, Figures 1–12 explain the variations of all the studied fields along the distance y and the distance x at $t = 0.3$. These figures display the predict curves during the strong, the weak and the normal conductivities. Unsurprisingly, you can find that the stages of the strong, normal and weak conductivities have great influences on the values of variables.

According to the fractional-order generalized thermoelastic model, we have to construct new classifications for all mediums according to their fractional parameter where these parameters become new indicators of their power to conduct thermal energy.

5. Conclusions

In this work, we studied the impacts of strong, weak, and normal thermal conductivities in porous materials under the generalized fractional-order thermoelastic model. The resulting nondimensional equations were solved by the Fourier–Laplace transformation method and, following that, applying the eigenvalue approach. The significant impacts of the strong, normal, and weak thermal conductivities were discussed for all physical quantities. Accordingly, generalized thermoelastic fractional-order models are considered as an advancement in the study of porous elastic materials.

Author Contributions: T.S. and I.A.A. have equally contributed to the elaboration of this manuscript. All authors have read and agreed to the published version of the manuscript.

Funding: This research received no external founding.

Institutional Review Board Statement: Not applicable.

Informed Consent Statement: Not applicable.

Data Availability Statement: Not applicable.

Conflicts of Interest: The authors declare no conflict of interest.

Appendix A

The matrix $A = [a_{ij}]$, $i, j = 1 \ldots 8$, and $a_{ij} = 0$ excepting

$a_{82} = \frac{r_{11} i q s^{\in+1}}{r_9+s}$, $a_{83} = \frac{r_{10} s^{\in}}{r_9+s}$, $a_{84} = q^2 + \frac{s^{\in+1}}{r_9+s}$, $a_{85} = \frac{s^{\in+1}\, r_{11}}{r_9+s}$,
$a_{72} = s_7 iq$, $a_{73} = s^2 r_4 + q^2 + r_6 + r_5 s$, $a_{74} = -r_8$, $a_{75} = r_7$,
$a_{62} = \frac{(s^2+q^2)}{r_1}$, $a_{63} = -\frac{r_2 iq}{r_1}$, $a_{64} = \frac{r_3 iq}{r_1}$, $a_{65} = -\frac{iq(1-r_1)}{r_1}$, $a_{51} = s^2 + r_1 q^2$, $a_{56} = -iq(1 - r_1)$, $a_{57} = -r_2$,
$a_{58} = r_3$, $a_{15} = a_{26} = a_{37} = a_{48} = 1$,
and $M = \left[\begin{array}{cccccccc} \overline{u}^* & \overline{v}^* & \overline{\varphi}^* & \overline{\Theta}^* & \frac{d\overline{u}^*}{dx} & \frac{d\overline{v}^*}{dx} & \frac{d\overline{\varphi}^*}{dx} & \frac{d\overline{\Theta}^*}{dx} \end{array} \right]^T$.

Appendix B

$f_1 = a_{58}a_{85} + a_{56}a_{65} + a_{57}a_{75} + a_{51} + a_{62} + a_{84} + a_{73}$,
$f_2 = a_{56}a_{65}a_{84} + a_{51}a_{73} - a_{74}a_{83} + a_{58}a_{62}a_{85} - a_{57}a_{74}a_{85} + a_{51}a_{84} + a_{57}a_{75}a_{84} - a_{56}a_{64}a_{85} + a_{58}a_{73}a_{85} + a_{62}a_{73} + a_{56}a_{65}a_{73} - a_{58}a_{75}a_{83} + a_{57}a_{62}a_{75} - a_{56}a_{63}a_{75} + a_{51}a_{62} - a_{63}a_{72} - a_{57}a_{65}a_{72} - a_{64}a_{82} - a_{58}a_{65}a_{82} + a_{62}a_{84} + a_{73}a_{84}$,
$f_3 = a_{56}a_{64}a_{73}a_{85} + a_{57}a_{65}a_{72}a_{84} + a_{56}a_{63}a_{75}a_{84} + a_{57}a_{62}a_{74}a_{85} - a_{56}a_{65}a_{73}a_{84} - a_{57}a_{62}a_{75}a_{84} - a_{58}a_{63}a_{75}a_{82} - a_{58}a_{65}a_{72}a_{83} + a_{51}a_{64}a_{82} + a_{64}a_{73}a_{82} + a_{58}a_{65}a_{73}a_{82} + a_{51}a_{74}a_{83} + a_{62}a_{74}a_{83} - a_{63}a_{74}a_{82} - a_{57}a_{65}a_{74}a_{82} + a_{63}a_{72}a_{84} - a_{56}a_{64}a_{75}a_{83} - a_{51}a_{62}a_{84} + a_{57}a_{64}a_{75}a_{82} - a_{64}a_{72}a_{83} - a_{51}a_{62}a_{73} + a_{58}a_{63}a_{72}a_{85} - a_{57}a_{64}a_{72}a_{85} - a_{58}a_{62}a_{73}a_{85} - a_{51}a_{73}a_{84} - a_{62}a_{73}a_{84} + a_{56}a_{65}a_{74}a_{83} + a_{58}a_{62}a_{75}a_{83} - a_{56}a_{63}a_{74}a_{85} + a_{51}a_{63}a_{72}$,
$f_4 = a_{51}a_{64}a_{72}a_{83} + a_{51}a_{62}a_{73}a_{84} - a_{51}a_{64}a_{73}a_{82} + a_{51}a_{63}a_{74}a_{82} - a_{51}a_{62}a_{74}a_{83} - a_{51}a_{63}a_{72}a_{84}$.

Appendix C

$Y_4 = -a_{58}\xi\left(\xi^6 + a_{51}\left(a_{63}a_{72} - \xi^4 + \left(\xi^2 - a_{73}\right)a_{62} + a_{73}\xi^2\right) - \xi^2\left((a_{57}a_{65} + a_{63})a_{72} + a_{73}\xi^2 + a_{57}a_{75}\xi^2 - a_{62}(a_{57}a_{75} - \xi^2 + a_{73}\right) + a_{56}\left(a_{75}a_{63} + \left(\xi^2 - a_{73}\right)a_{65}\right)\right)\right)$,
$Y_3 = -\xi a_{58}\left(\left(\left(-\xi^2 + a_{62}\right)\left(-\xi^2 + a_{51}\right) - \xi^2 a_{65}a_{56}\right)a_{74} + \left(a_{72}\left(\xi^2 - a_{51}\right) + \xi^2 a_{75}a_{56}\right)a_{64} + a_{58}\xi^2\left(\left(\xi^2 - a_{62}\right)a_{75} + a_{72}a_{65}\right)\right)$,
$Y_2 = -\xi(a_{63}a_{58} - a_{64}a_{57})\left(\left(-a_{51} + \xi^2\right)a_{74} + \xi^2 a_{75}a_{58}\right) - \xi\left(a_{64}\left(\xi^2 - a_{51}\right) + \xi^2 a_{65}a_{58}\right)\left(a_{57}a_{74} + a_{58}\left(\xi^2 - a_{73}\right)\right)$,
$Y_1 = -\left(\xi a_{58}\left(a_{62} - \xi^2\right) - \xi a_{64}a_{56}\right)\left(\xi a_{58}\left(a_{73} - \xi^2\right) - \xi a_{74}a_{57}\right) + \xi^2(-a_{57}a_{64} + a_{58}a_{63})(-a_{56}a_{74} + a_{58}a_{72})$,
$Y_5 = Y_1\xi$, $Y_6 = Y_2\xi, Y_7 = Y_3\xi, Y_8 = Y_4\xi$,

References

1. Biot, M.A. Thermoelasticity and irreversible thermodynamics. *J. Appl. Phys.* **1956**, *27*, 240–253. [CrossRef]
2. Rosencwaig, A.; Opsal, J.; Willenborg, D.L. Thin-film thickness measurements with thermal waves. *Appl. Phys. Lett.* **1983**, *43*, 166–168. [CrossRef]
3. Biot, M.A. General solutions of the equations of elasticity and consolidation for a porous material. *J. Appl. Mech.* **1956**, *23*, 91–96.
4. Biot, M.A. Theory of propagation of elastic waves in a fluid-saturated porous solid. II. Higher frequency range. *J. Acoust. Soc. Am.* **1956**, *28*, 179–191. [CrossRef]
5. Lord, H.W.; Shulman, Y. A generalized dynamical theory of thermoelasticity. *J. Mech. Phys. Solids* **1967**, *15*, 299–309. [CrossRef]
6. Green, A.E.; Naghdi, P.M. A re-examination of the basic postulates of thermomechanics. *Proc. R. Soc. Lond. Ser. A Math. Phys. Sci.* **1991**, *432*, 171–194.
7. Green, A.; Naghdi, P. On undamped heat waves in an elastic solid. *J. Therm. Stresses* **1992**, *15*, 253–264. [CrossRef]
8. Green, A.; Naghdi, P. Thermoelasticity without energy dissipation. *J. Elast.* **1993**, *31*, 189–208. [CrossRef]
9. Youssef, H.M. Theory of fractional order generalized thermoelasticity. *J. Heat Transf.* **2010**, *132*, 061301. [CrossRef]
10. Youssef, H.M.; Al-Lehaibi, E.A. Variational principle of fractional order generalized thermoelasticity. *Appl. Math. Lett.* **2010**, *23*, 1183–1187. [CrossRef]
11. Sherief, H.H.; El-Sayed, A.M.A.; Abd El-Latief, A.M. Fractional order theory of thermoelasticity. *Int. J. Solids Struct.* **2010**, *47*, 269–275. [CrossRef]
12. Ezzat, M.A.; El Karamany, A.S. Theory of fractional order in electro-thermoelasticity. *Eur. J. Mech. A Solids* **2011**, *30*, 491–500. [CrossRef]
13. Ezzat, M.; El-Karamany, A.; El-Bary, A. Modeling of memory-dependent derivative in generalized thermoelasticity. *Eur. Phys. J. Plus* **2016**, *131*, 372. [CrossRef]
14. Marin, M. Some basic theorems in elastostatics of micropolar materials with voids. *J. Comput. Appl. Math.* **1996**, *70*, 115–126. [CrossRef]
15. Saeed, T.; Abbas, I.; Marin, M. A GL Model on Thermo-Elastic Interaction in a Poroelastic Material Using Finite Element Method. *Symmetry* **2020**, *12*, 488. [CrossRef]
16. Ouyang, X.L.; Xu, R.N.; Jiang, P.X. Three-equation local thermal non-equilibrium model for transient heat transfer in porous media: The internal thermal conduction effect in the solid phase. *Int. J. Heat Mass Transf.* **2017**, *115*, 1113–1124. [CrossRef]
17. Abbas, I.A. The effects of relaxation times and a moving heat source on a two-temperature generalized thermoelastic thin slim strip. *Can. J. Phys.* **2015**, *93*, 585–590. [CrossRef]
18. Zenkour, A.M.; Abbas, I.A. Magneto-thermoelastic response of an infinite functionally graded cylinder using the finite element method. *J. Vib. Control* **2014**, *20*, 1907–1919. [CrossRef]
19. Abbas, I.A. Nonlinear transient thermal stress analysis of thick-walled FGM cylinder with temperature-dependent material properties. *Meccanica* **2014**, *49*, 1697–1708. [CrossRef]
20. El-Naggar, A.M.; Kishka, Z.; Abd-Alla, A.M.; Abbas, I.A.; Abo-Dahab, S.M.; Elsagheer, M. On the initial stress, magnetic field, voids and rotation effects on plane waves in generalized thermoelasticity. *J. Comput. Theor. Nanosci.* **2013**, *10*, 1408–1417. [CrossRef]
21. Sur, A.; Mondal, S. A generalized thermoelastic problem due to nonlocal effect in presence of mode I crack. *J. Therm. Stresses* **2020**, *43*, 1277–1299. [CrossRef]
22. Othman, M.I.; Mondal, S. Memory-dependent derivative effect on wave propagation of micropolar thermoelastic medium under pulsed laser heating with three theories. *Int. J. Numer. Methods Heat Fluid Flow* **2019**, *30*, 1025–1046. [CrossRef]
23. Abbas, I.A.; El-Amin, M.; Salama, A. Effect of thermal dispersion on free convection in a fluid saturated porous medium. *Int. J. Heat Fluid Flow* **2009**, *30*, 229–236. [CrossRef]
24. Hussein, E.M. Mathematical Model for Thermoelastic Porous Spherical Region Problems. *Comput. Therm. Sci. Int. J.* **2020**, *12*, 233–248. [CrossRef]
25. Hobiny, A.; Abbas, I. Generalized thermoelastic interaction in a two-dimensional porous medium under dual phase lag model. *Int. J. Numer. Methods Heat Fluid Flow* **2020**, *30*, 4865–4881. [CrossRef]
26. Biswas, S. Surface waves in porous nonlocal thermoelastic orthotropic medium. *Acta Mech.* **2020**, *231*, 2741–2760. [CrossRef]
27. Carini, M.; Zampoli, V. On porous matrices with three delay times: A study in linear thermoelasticity. *Mathematics* **2020**, *8*, 371. [CrossRef]
28. Abbas, I.A.; Marin, M. Analytical Solutions of a Two-Dimensional Generalized Thermoelastic Diffusions Problem Due to Laser Pulse. *Iran. J. Sci. Technol. Trans. Mech. Eng.* **2018**, *42*, 57–71. [CrossRef]
29. Shekhar, S. Study of deformation due to thermal shock in porous thermoelastic material with reference temperature dependent properties. *Mech. Based Des. Struct. Mach.* **2020**. [CrossRef]
30. Itu, C.; Öchsner, A.; Vlase, S.; Marin, M.I. Improved rigidity of composite circular plates through radial ribs. *Proc. Inst. Mech. Eng. Part L J. Mater. Des. Appl.* **2019**, *233*, 1585–1593. [CrossRef]
31. Abd-Elaziz, E.M.; Marin, M.; Othman, M.I. On the effect of Thomson and initial stress in a thermo-porous elastic solid under GN electromagnetic theory. *Symmetry* **2019**, *11*, 413. [CrossRef]

32. Abbas, I.A.; Kumar, R. Deformation due to thermal source in micropolar generalized thermoelastic half-space by finite element method. *J. Comput. Theor. Nanosci.* **2014**, *11*, 185–190. [CrossRef]
33. Sheikholeslami, M.; Ellahi, R.; Shafee, A.; Li, Z. Numerical investigation for second law analysis of ferrofluid inside a porous semi annulus: An application of entropy generation and exergy loss. *Int. J. Numer. Methods Heat Fluid Flow* **2019**, *29*, 1079–1102. [CrossRef]
34. Ellahi, R.; Sait, S.M.; Shehzad, N.; Ayaz, Z. A hybrid investigation on numerical and analytical solutions of electro-magnetohydrodynamics flow of nanofluid through porous media with entropy generation. *Int. J. Numer. Methods Heat Fluid Flow* **2019**, *30*, 834–854. [CrossRef]
35. Singh, B. Wave propagation in a generalized thermoelastic material with voids. *Appl. Math. Comput.* **2007**, *189*, 698–709. [CrossRef]
36. Palani, G.; Abbas, I. Free convection MHD flow with thermal radiation from an impulsively started vertical plate. *Nonlinear Anal. Model. Control* **2009**, *14*, 73–84. [CrossRef]
37. Villatoro, F.R.; Pérez, J.; Santander, J.L.G.; Borovsky, M.A.; Ratis, Y.L.; Izzheurov, E.A.; de Córdoba, P.F. Perturbation analysis of the heat transfer in porous media with small thermal conductivity. *J. Math. Anal. Appl.* **2011**, *374*, 57–70. [CrossRef]
38. Abbas, I. Natural frequencies of a poroelastic hollow cylinder. *Acta Mech.* **2006**, *186*, 229–237. [CrossRef]
39. Alzahrani, F.; Hobiny, A.; Abbas, I.; Marin, M. An Eigenvalues Approach for a Two-Dimensional Porous Medium Based Upon Weak, Normal and Strong Thermal Conductivities. *Symmetry* **2020**, *12*, 848. [CrossRef]
40. Hobiny, A.; Alzahrani, F.; Abbas, A.; Marin, M. The Effect of fractional time derivative of bioheat model in skin tissue induced to laser irradiation. *Symmetry* **2020**, *12*, 602. [CrossRef]
41. Das, N.C.; Lahiri, A.; Giri, R.R. Eigenvalue approach to generalized thermoelasticity. *Indian J. Pure Appl. Math.* **1997**, *28*, 1573–1594.
42. Abbas, I.A.; Alzahrani, F.S.; Elaiw, A. A DPL model of photothermal interaction in a semiconductor material. *Waves Random Complex Media* **2019**, *29*, 328–343. [CrossRef]
43. Saeed, T.; Abbas, I. Thermomechanical response in a two-dimension porous medium subjected to thermal loading. *Int. J. Numer. Methods Heat Fluid Flow* **2019**, *30*, 4103–4117. [CrossRef]
44. Stehfest, H. Algorithm 368: Numerical inversion of Laplace transforms [D5]. *Commun. ACM* **1970**, *13*, 47–49. [CrossRef]
45. Othman, M.I.; Marin, M. Effect of thermal loading due to laser pulse on thermoelastic porous medium under GN theory. *Results Phys.* **2017**, *7*, 3863–3872. [CrossRef]